# PHYSICAL AND CHEMICAL CHARACTERIZATION OF CHINESE FALLEN POPLAR LEAF ASH: EFFECTS OF THE CALCINING TEMPERATURE AND AQUEOUS SOLUTION

*Tingye Qi*
Associate Professor
College of Mining Technology
Taiyuan University of Technology
Taiyuan 030024, P. R. China
State Key Laboratory of Coal Resources and Safe Mining
China University of Mining and Technology
Xuzhou 030024, P. R. China
and
Shanxi Province Research Center of Green Mining Engineering Technology
Taiyuan University of Technology
Taiyuan 030024, P. R. China
E-mail: qty198402@163.com

*Shufeng Zhang*
Master
E-mail: zsf1741@163.com

*Guorui Feng**
Professor
College of Mining Technology
Taiyuan University of Technology
Taiyuan City 030024, P. R. China
and
Shanxi Province Research Center of Green Mining Engineering Technology
Taiyuan University of Technology
Taiyuan 030024, P. R. China
E-mail: fgr09000@126.com

*Guang Xu*
Lecture
Department of Mining Engineering and Metallurgical Engineering
Western Australian School of Mines
Curtin University
95 Egan Street
Kalgoorlie, Australia 6430
E-mail: 340449868@qq.com

(Received February 2019)

**Abstract.** This study focused on the physical and chemical characterization of Chinese poplar leaf ash (PLA) with 500°C, 700°C, and 850°C calcination temperatures and residual PLA leaching from aqueous solution. The grain size distribution, chemical composition, and microstructure of PLA were investigated by laser granulometric distribution, X-ray fluorescence, and scanning electron microscopy. The ash samples obtained before and after aqueous dissolution were analyzed using X-ray powder diffraction to identify the mineral components. X-ray photoelectron spectroscopy was used to illustrate the Si 2p and Al 2p

* Corresponding author

*Wood and Fiber Science*, 51(3), 2019, pp. 309-319
https://doi.org/10.22382/wfs-2019-029

transformation behaviors in the PLA samples. The zeta potentials, conductivities, and pH values of hybrid solutions were tested at different dissolution times. Silica, sulfur, calcium, and potassium were the dominant components observed in the PLA. The conductivities and pH values were nearly stable with an increasing dissolution time. The zeta potential of PLA was calculated to be a negative value. Calcite and potassium sulfate were found in the PLA-500 and PLA-700 samples, whereas magnesite and lime were easily identified in PLA-850. The Si 2p peak shifted to a lower position because of the additional synthesis of Si-OH with the increasing calcination temperature. These conclusions could help investigations into the possibility of using PLA in cement systems.

***Keywords:*** Poplar leaf ash, calcining temperature, aqueous solution, Si 2p, Al 2p.

## INTRODUCTION

Woody biomass can be used to produce electricity energy through direct combustion (Bridgwater 2006). In North America and Europe, cellulosic biomass used for bioenergy production is mainly derived from short-rotation willow and poplar coppice cultures (Liu et al 2009; Evangelou et al 2012). In North China, a large quantity of fallen woody biomass leaves, such as poplar leaves, are produced every year. However, these biomass energy sources are either buried underground or directly discarded as waste, and applications of biomass have great potential. However, if woody biomass leaves are used for energy, the Chinese society faces questions regarding how to deal with large amounts of poplar leaf ash (PLA). In this context, the physical and chemical characteristics of PLA were studied. The information is helpful for dealing with a mass of PLA.

Si and Al are the main chemical elements in the earth and are also the component elements of biomass, geopolymers, and cement-based materials. Prior reports stated that minerals and phases containing Si and Al would be transformed during the combustion of biomass ash (BA), especially agricultural biomass. Preparation of more active amorphous silica from rice husks depended on the presence of totally crystalline silica in the original rice husk ash prepared at 800°C, leaching procedure, low calcination temperature, and short calcination time (Shen et al 2011). Both the porosity of lemon grass ash and the crystallinity of silica in lemon grass ash increased as the calcination temperature increased from 0 to 700°C (Firdaus et al 2016). Bamboo leaves burned in an open atmosphere and then heated at 600°C for 2 h in a furnace were found to produce an amorphous material containing amorphous silica (Dwivedi et al 2006). In addition, based on prior studies (Vassilev et al 2013a), biomass could produce different Al-containing elements, minerals, and phases during the combustion procedure. For example, elemental Al, K-Al sulfate, K aluminosilicate, and albite appeared at 660°C, 690-800°C, 695°C, and 1118°C calcination temperatures, respectively. K-feldspars, microcline, orthoclase, and sanidine appeared at 1170°C calcination temperature, whereas biotite, chlorite, and muscovite appeared at 1200°C calcination temperature.

Based on the abovementioned references, amorphous silica can be produced using calcination procedures and is a very useful material from biomass that reacts with calcium hydroxide to produce C-S-H. Therefore, BAs, such as palm oil clinker powder, wheat straw ash, sugar cane bagasse ash, and sugar cane straw ash (Biricik et al 1999; Cociña et al 2013; Karim et al 2016), are usually added to cement-based materials (Moraes et al 2015) to improve their strength (Dwivedi et al 2006).

For woody biomass, such as willow, Vassilev (2013b) concluded that the temperatures of the initial deformation, spherical morphology, hemispherical morphology, and fluid phase for willow stem ash are 1453°C, 1518°C, 1528°C, and 1550°C, respectively. Qu et al (2015) found that willow leaves heated to 500°C could synthesize carbon nanospheres and adsorb rhodamine B and heavy metals. Another woody biomass, poplar leaves, is usually used to prepare biochar; Bai et al (2017) used corn straw and poplar leaves to prepare biochar with different pyrolysis temperatures and found that two biochars possessed

similar characteristics with increasing pyrolysis temperature, including elemental analysis, ash content, and pH. Akhtar et al (2016) investigated the physicochemical characteristics of leaf litter from large tree species such as *Populus deltoides*. Low ash content and high volatile matter were observed from *P. deltoides* leaves. A fibrillar structure and a maximum crystallinity index were observed in the *P. deltoides* leaf, and the study concluded that the leaf litter of *P. deltoides* can also act as a potential feedstock for biofuel production. However, few reports of Si and Al transformations during the combustion of the populus leaf are available.

Water is the primary component of cement-based materials, and therefore, the water solubility and reactivity of PLA should be investigated. Some studies showed that the water-soluble phases of BA mostly include alkali and alkaline earth elements: 1) highly soluble phases (chlorides, sulfates, oxides, hydroxides, nitrates, carbonates, and bicarbonates); 2) certain less-soluble phases (carbonates, phosphates, and oxides); and 3) some slightly soluble phases (phosphates and silicates) (Vassilev et al 2014). Moreover, water-soluble phases could transform to more stable acid-soluble and acid-insoluble forms (Jordan and Akay 2012).

Reference investigations also showed that the content of water-soluble fractions in BA is high (Baxter et al 1998; Van et al 2008) and can be up to 61.0% (Lima et al 2008). The pH values of biomass to be investigated and the soluble Ca, Mg, K, and Na hydroxides, oxides, carbonates, and bicarbonates in BA are also responsible for high pH in BA (Steenari et al 1999). At the same time, it was found that pH values of woody BAs are higher than those of cereal and straw BAs because of the higher Ca and lower S and Cl concentrations in the woody ashes (Etiegnit et al 1991; Ulery et al 1993; Demeyer et al 2001).

In this study, the composition and microstructure of PLA at 500°C, 700°C, and 850°C calcination temperatures were investigated. The pH values, conductivities, and zeta potentials were measured after mixing the PLA in deionized water for 0-2 h. The mineralogy and Si 2p and Al 2p chemical bonds of the PLA samples and water-leaching residues were investigated. This knowledge is essential for understanding the influence of calcination temperature on the characteristics of PLA and for determining the water-leaching properties of PLA. These conclusions could be helpful for assessing the possibility of PLA use in cement systems.

## MATERIALS AND METHODS

Fallen poplar leaf samples were collected from the Taiyuan city suburb, Shanxi province, China, in autumn. The samples were washed using tap water to remove impurities, dried at 105°C for 24 h in a circulating oven, crushed to a 1-cm grain size, and placed into a muffle furnace to calcine for 3 h at 500°C (PLA-500), 700°C (PLA-700), and 850°C (PLA-850). The cooled PLA was milled by sealing the sample preparation machine and was filtered using a 0.074-mm membrane filter. The samples were characterized by laser granulometric distribution, X-ray photoelectron spectroscopy (XPS), scanning electron microscopy (SEM), and X-ray powder diffraction (XRD). The samples from the three calcination temperatures were dissolved in deionized water at a liquid-to-solid (L/S) ratio of 2/15 L/g, and pH values and conductivities of the solutions were tested at 15-min intervals during the 2-h dissolution time. The zeta potentials were measured at 30-, 60-, and 90-min dissolution times. The residues after leaching at 15 min and 2 h were dried in the oven at 80°C, and XRD analysis was carried out on the dried residues. Ordinary Portland cement (OPC) was also dissolved in deionized water at an L/S ratio of 2/15 L/g to test the zeta potential for comparison with the PLA samples.

The grain size distribution (GSD) of PLA can affect the resultant paste consistency, chemical reactivity, and the overall hydromechanical properties (Feng et al 2018). The GSD curves of the PLA samples were determined using a Malvern Laser Mastersizer S 2000 (Malvern Instruments Inc., Worcestershire, UK) with an accuracy of $\pm 1\%$.

The main chemical composition of PLA (in the form of oxides) was determined by XRF (ZSX Primus II; Rigaku Corp., Tokyo, Japan). The samples were disposed according to GB/T 28731 (2012) and GB/T 30726 (2014).

The microstructure analysis of PLA samples was performed using a JEOL JSM 6390 LV (JEOL Ltd., Tokyo, Japan) electron microscope at 25 kV. The samples were previously Au-coated (SKY Technology Development Corp., Shenyang, China) to avoid charging problems.

The minerals of PLA and PLA residuals were characterized by X-ray powder diffractometry using an Ultima IV Rigaku diffractometer (Rigaku Corp.) equipped with Cu Kα1, 2 ($\lambda$ = 1.54178 Å) radiation with a generator voltage of 40.0 kV and a current of 40.0 mA. The 2θ range of 5°-90° was used for all powders in continuous scan mode with a scanning step of 0.02° at a rate of 10°/min.

Zeta potentials in the aqueous solutions of PLA and OPC were characterized using a microscopic electrophoresis apparatus (JS94H; Powereach Corp., Shanghai, China) with a Ag electrode. The measurement parameters were as follows: particle size range of 0.5 to 20 μm, input pH range of 1.6 to 13.0, step length of 0.1, and switching time of 700 ms. The pH and conductivity values of the solutions were measured using an LEICI PHSJ-3 pH meter and LEICI DDS-307A conductivity meter (INESA Scientific Instrument Co., Ltd., Shanghai, China), respectively. The pH and conductivity were tested three times, and the average values were obtained.

An XPS analysis for PLA was performed using an Axis Ultra DLD instrument (Kratos, Manchester, UK) for surface characterization. Photoelectron emission was excited via a monochromatic Al Kα line with an energy of 1486.67 eV. The powder samples were heated for approximately 2 h at 80°C in air to reduce the amount of adsorbed water. Immediately after removing them from the oven, the samples were fixed on adhesive tape and introduced into the vacuum system.

## RESULTS AND DISCUSSION

According to the GSD curves of the samples (<0.074 mm, Fig 1), the particle size of PLAs at different calcination temperatures exhibits nearly continuous gradation. Moreover, the specific surface area decreased, and the median particle diameter increased with increasing calcination temperature (Table 1).

As Table 1 shows, the loss on ignition increased with increasing calcination temperature. Depending on the combustion temperature, the chemical composition of PLA varies. Mostly, a higher proportion of silica, potassium oxide, magnesium oxide, and lime compounds was observed in the PLA composition. The abundance of K and Ca in PLA, together with the high Si content, favors the formation of alkali-rich silicates and, thus, decreases the ash melting temperature (Zhu et al 2018). Moreover, a high $SO_3$ content was found in the PLA samples, which means that more S content would be fixed in the form of $K_2SO_4$ in the PLA samples (as seen in the XRD results). The K and Cl contents for PLA-850 were the lowest of the three calcination temperature samples, which could be explained by the release of gas-phase KCl at 850°C from PLA (Knudsen et al 2004). Meanwhile, the contents of the refractory elements Na, Mg, Ca, Fe, Al, and Si, as well as S and P, are nearly constant or slightly higher with increased temperature. This augmentation could be attributed

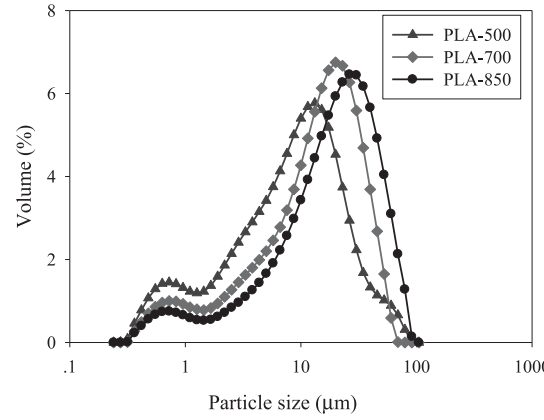


Figure 1. Grain size distribution of poplar leaf ash (PLA) at 500°C, 700°C, and 850°C calcination temperatures.

Table 1. Chemical composition of poplar leaves calcined at 500°C, 700°C, and 850°C.

| Sample | $SiO_2$ (%) | $Al_2O_3$ (%) | $Fe_2O_3$ (%) | CaO (%) | MgO (%) | $SO_3$ (%) | $TiO_2$ (%) | $K_2O$ (%) | $Na_2O$ (%) | $P_2O_5$ (%) | Cl (%) | LOI (%) | Specific surface area ($m^2/g$) | Median particle diameter (μm) |
|---|---|---|---|---|---|---|---|---|---|---|---|---|---|---|
| PLA-500 | 5.22 | 1.54 | 1.04 | 34.99 | 3.39 | 9.96 | 0.09 | 13.11 | 0.5 | 1.0 | 0.65 | 82.34 | 1.98 | 8.282 |
| PLA-700 | 4.33 | 1.35 | 0.97 | 37.08 | 3.67 | 10.85 | 0.08 | 13.75 | 0.56 | 1.08 | 0.65 | 85.56 | 1.38 | 13.584 |
| PLA-850 | 13.16 | 3.69 | 2.93 | 47.27 | 4.73 | 11.49 | 0.21 | 9.56 | 0.78 | 1.36 | 0.3 | 87.22 | 1.08 | 18.456 |

to an increase in the relative content of these elements with the release of volatile species. The augmentation of Mg, Ca, P, and S contents in the ash implies that more high–melting-temperature substances are formed (Bostrom et al 2012).

Figures 2 and 3 show the relationship between conductivity and dissolution time and the relationship between pH value and dissolution time of PLA after treatment at 500°C, 700°C, and 850°C and mixing in an aqueous solution, respectively. When PLAs from different calcination temperatures were dissolved in deionized water, the pH of the aqueous solution was greater than 10.8 for the duration of the dissolution time, from 0 to 120 min. The high levels of $K_2O$ and CaO are responsible for the high alkalinity of the water medium (Font et al 2017), and these compounds are also identified in the PLA (especially in PLA-700 and PLA-850, as seen from XRD). The sequence of pH values and conductivities appeared to follow PLA-850 > PLA-700 > PLA-500 at all dissolution times, showing more active ions and $OH^-$ in the PLA-850 aqueous solution. More soluble minerals (eg CaO and $K_2SO_4$) were found in PLA-850; CaO could react with $H_2O$ to produce $Ca(OH)_2$, which leads to the higher pH value.

The pH values changed slightly with increasing dissolution time, which indicated minimal consumption of $OH^-$ participating in chemical reactions in the PLA aqueous solutions. For PLA-850, the conductivity value decreased with the increasing dissolution time, which indicated that the total ion concentration declined with the dissolution time. For PLA-700, the conductivity slightly decreased with the increasing dissolution time. Compared with samples treated by relatively high temperature, the conductivity changes of PLA-500 were not obvious. These results indicated small variations in ion concentrations in PLA-500 and PLA-700 during dissolution in the aqueous solution.

To determine the role of surface charge on repulsion, the zeta potentials of PLA samples were calculated and were found to be negative values (as shown in Table 2). This result indicates that

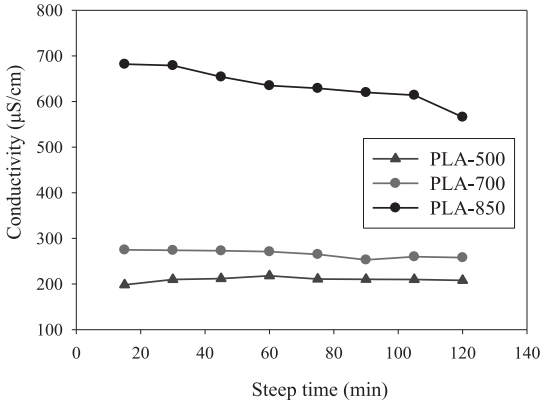


Figure 2. Relationship between the conductivity and dissolution time of poplar leaf ash (PLA) after treatment at 500°C, 700°C, and 850°C and mixing in an aqueous solution.

the surface of PLA particles has a moderately negative charge. The surface of PLA particles is rich with oxides of $SiO_2$; the available negative charge sites of the silica surface are dominated in high pH. Moreover, the presence of oxygen and carbon in PLA contains functional groups such as carboxylic groups. This functional group (COO−) has negative surface charge and can increase the cation exchange capacity of the adsorbent (Hafshejani et al 2015). An electronegative surface of PLA particles can be beneficial for repulsion of anion-like cement.

The zeta potential for PLA-850 changes slightly with increasing dissolution time because of the

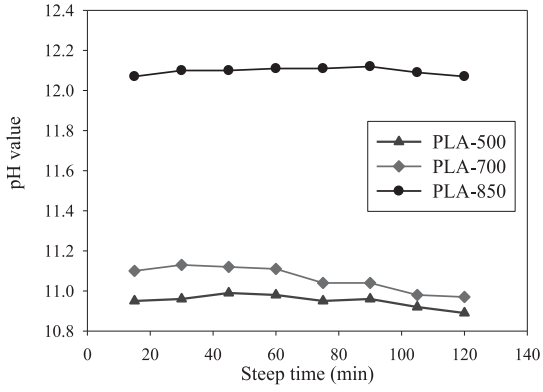


Figure 3. Relationship between pH value and dissolution time of poplar leaf ash (PLA) after treatment at 500°C, 700°C, and 850°C and mixing in an aqueous solution.

Table 2. Zeta potential (mV) of PLA calcined at 500°C, 700°C, and 850°C after dissolving in aqueous solution for 30, 60, and 90 min.

| | Steep time (min)/zeta potential (eV) | | |
|---|---|---|---|
| Sample | 30 | 60 | 90 |
| PLA-500 | −1.228 | −12.651 | −10.389 |
| PLA-700 | −10.156 | −14.781 | −6.966 |
| PLA-850 | −7.514 | −9.127 | −8.817 |
| OPC | −12.570 | −25.854 | −15.546 |

PLA, poplar leaf ash.

relatively stable pH value of the aqueous solution. The zeta potentials for PLA-500 and PLA-700 first increase and then decrease as the dissolution time increases. Early in dissolution, the particle surfaces constantly absorb anions from the mixing solution, which adds to the negative charge. This process may explain the increase in zeta potentials over the interval from 30 to 60 min. With increasing dissolution time, the K and Ca ions could react with $OH^-$ existing on the surface of the PLA particles, producing new minerals that surround the particles and cause a charged double layer that is compressed by electrostatic interactions. This may explain the decline in zeta potentials in the interval from 60 to 90 min (Moghal and Sivapullaiah 2012).

Although the negatively charged surface of PLA is the same as OPC particles, the zeta potential values of PLA are less than those of OPC. The repulsive force is limited, and adding PLA to the cement system to improve the flowability of the slurry for the cementing materials is not recommended (Givi et al 2010).

Microphotographs reveal that some irregularly shaped materials appeared at the surface of PLA-500 particles (Fig 4(a)). As the thermal temperature increased, the quantity of the irregularly shaped materials decreased. More compact structures were observed in PLA samples, and these behaviors indicated an incipient sinterization process. The SEM images obtained confirm particle aggregation when poplar leaf samples were thermally treated. Compared with PLA at 700°C (Fig 4(b)) and 500°C, larger numbers of agglomerated particles were observed on the surface of the PLA sample treated at 850°C. The

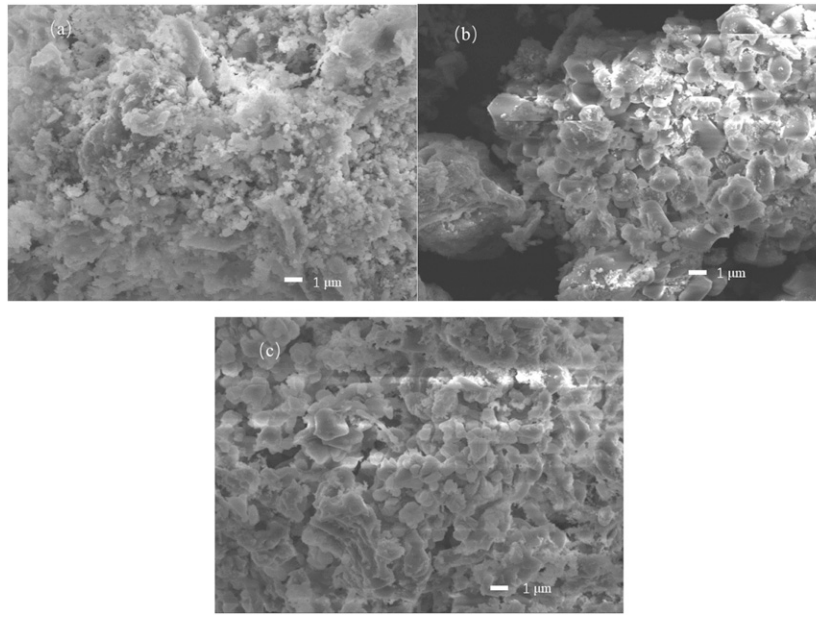


Figure 4. Scanning electron microscopy images of poplar leaf ash at different calcined temperatures: 500°C (a); 700°C (b); and 850°C (c).

aggregation phenomenon is related to the production of alkali silicate minerals at 850°C (Fig 4(c)). Moreover, the SEM results corroborate the grain size results that bigger PLA particle sizes correspond to higher calcination temperatures.

Figure 5 shows the major minerals in the PLA samples with different calcination temperatures and in all the different calcination temperature residue samples with 15- and 120-min dissolution times. From Fig 5(a) and (b), calcite and potassium sulfate can be found in the PLA-500 and PLA-700 samples. At the calcination temperature of 850°C (Fig 5(c)), $CaCO_3$ disappeared, decomposing to CaO and $CO_2$. Magnesite is easily identified in the PLA-850. Crystalline Al- and Si-containing minerals are hardly identifiable in the PLA samples.

When the PLA-500 and PLA-700 samples dissolved in the aqueous solution, soluble minerals, such as potassium sulfate, disappeared from the XRD results. Insoluble minerals, such as calcite, remain in the PLA residue samples and do not vary with dissolution time (as seen from Fig 5(a) and (b)).

Table 3 shows the major analysis for Si- and Al-containing minerals in the PLA-850 residue samples after dissolving for 15 and 120 min, which could not be found in the PLA-850 sample (Fig 5(c)). This phenomenon could be explained in two ways. One explanation is that during the process of PLA calcinated at 850°C, some amorphous $SiO_2$ would be produced; the $SiO_2$ is able to incorporate with an interstitial cation, such as $Na^+$, $K^+$, or $Ca^{2+}$, in the hollow regions of six-membered tetrahedral $SiO_{4/2}$. The productions of silicate minerals were formed. These inclusions mainly involve the valence of compensation elements, requiring an open structure for crystalline phase transformations (Soltani et al 2015). These Si- and Al-containing minerals are deposited in the middle of the PLA samples. Soluble materials exist on the surface of PLA samples dissolved in aqueous solution, such as potassium sulfate and lime, and these Al- and Si-containing minerals would be exposed at the surface of the particles and could be identified by XRD.

The other possible explanation is that the surface of PLA is negatively charged (as seen from the

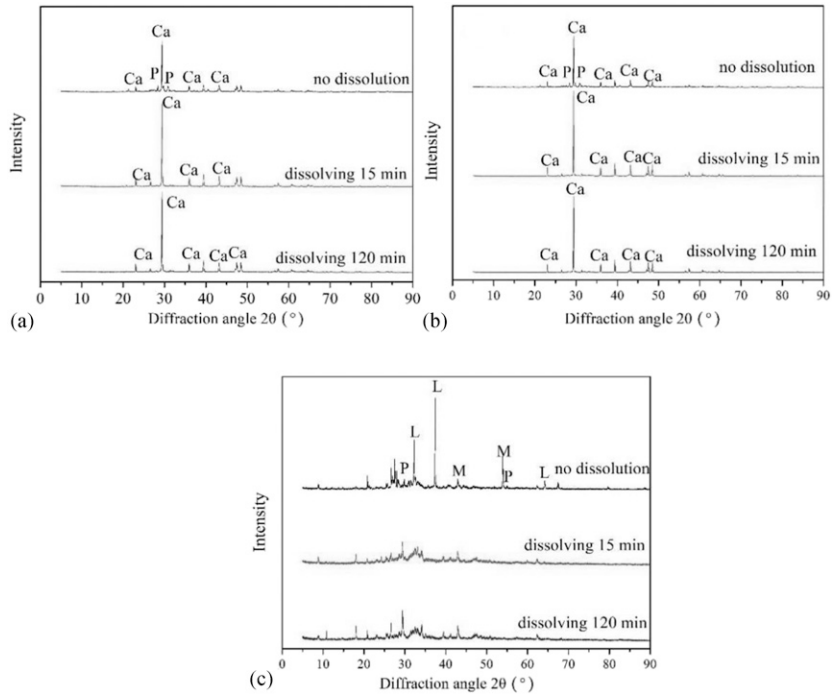


Figure 5. X-ray powder diffraction patterns for PLA-500 (a), PLA-700 (b), and PLA-850 (c) for no dissolution and dissolving for 15 and 120 min; key for major minerals: Ca-Calcite ($CaCO_3$); P-potassium sulfate ($K_2SO_4$); M-magnesite ($MgCO_3$); and L-lime (CaO).

zeta potential results) so that precipitate chemical reactions happened during the dissolution process. Furthermore, the metals are adsorbed in PLA by a strong tendency toward chemical bonding between the metal groups and the oxide surface (Liu et al 2018). The silicate precursors were formed in situ by dissolution of amorphous silica particles by an alkaline solution (Simonsen et al 2009). However, the reaction degree is very low, as can be proven from the pH values and conductivities of PLA-850 dissolved in aqueous solution.

XPS is a widely applicable tool to probe surface chemical compositions and atomic structure environments. Figure 6(a) and (b) shows the fitting of

Table 3. Major minerals in the PLA-850 residue after 15- and 120-min dissolving time.

| Sample | Minerals | Diffraction angle (°) |
|---|---|---|
| PLA-850 residue after dissolving for 15 min | Tobermorite $Ca_5(Si_6O_{16})(OH)_2$ | 11.156, 7.303, 9.566 |
| | Biotite $KFeMg_2(AlSi_3O_{10})(OH)_2$ | 5.337, 9.242, 10.211 |
| | Fluorphlogopite $K_{0.86}Mg_{2.31}Li_{0.69}Al_{0.16}Si_{3.84}O_{10}F_2$ | 5.310, 9.190, 40.580 |
| | Phlogopite $KMg_3AlSi_3O_{10}OHF$ | 5.30, 9.20, 20.20 |
| | Annite $K_2(Fe5+2Al)Si_5Al_3O_{20}(OH)_4$ | 5.369, 9.297, 10.268 |
| | Larnite $Ca_2(SiO_4)$ | 5.502, 6.762, 9.339 |
| PLA-850 residue after dissolving for 120 min | Quartz $SiO_2$ | 4.914, 5.404 |
| | Merwinite $Ca_3Mg(SiO_4)_2$ | 9.336, 5.301, 13.286 |
| | Biotite $K[Mg, Fe]_3Al(Si_3O_{10})F_2$ | 5.329, 9.230, 10.219 |
| | Phlogopite $KMg_3(Si_3Al)O_{10}(OH)_2$ | 5.329, 9.234, 20.098 |

PLA, poplar leaf ash.

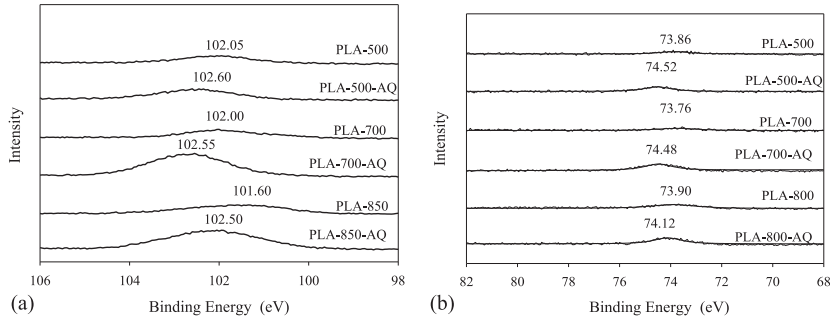


Figure 6. Si 2p (a) and Al 2p (b) line shifts of PLA at 500°C, 700°C, and 850°C calcination temperatures.

Si 2p and Al 2p lines, respectively, taken from PLA samples with different calcination temperatures.

As Fig 6(a) shows, the binding energy peaks of Si 2p lines for PLA-500, PLA-700, and PLA-850 are situated at approximately 102.8, 101.75, and 101.4 eV, respectively. The peak position of Si 2p lines appeared at a lower position with increasing calcination temperature because the Si bond is transformed after calcination of PLA samples. The Si 2p lines in PLAs with different calcination temperatures could be resolved into different contributions, which means that Si 2p in PLA can be made up of different chemical bonds, such as Si-O-Si, Si-OH, and $SiO_2$.

The Si 2p line in PLA-500 depends on the silica because of the high peak position with a distribution from 103.1 to 103.8 eV (Paparazzo et al 1992); a possible candidate would be amorphous opal because crystalline silica was not found in PLA-500 by XRD. When the calcination temperature is 700°C, some amorphous $SiO_2$ would transform the relatively stable framework silicate structure, namely, quartz. The other amorphous $SiO_2$ would synthesize silicate minerals, namely, merwinite. The Si-O-Si and Si-OH bonds located at a low peak position, ~101.0-102.6 eV, are responsible for the lower position of the Si 2p line in the PLA-700 sample. When the calcination temperature is 850°C, more Si-OH had been synthesized, which led to the lower peak position of Si 2p than for the PLA-700 sample (Ljiljana et al 2017).

Under alkaline conditions, the surface silanols interact with $OH^-$ to form negatively charged surface species via protonation (Eq 1) (Zhu et al 2017):

$$> \mathrm{SiOH} + \mathrm{OH}^- = > \mathrm{SiO}^- + \mathrm{H_2O}, \quad (1)$$

where $> \mathrm{SiOH}$ and $> \mathrm{SiO}^-$ stand for the neutral and deprotonated surface sites, respectively.

The characteristics of surface sites could significantly affect the solubility and reaction mechanisms of silica minerals. Greater $> \mathrm{SiO}^-$ structure could be responsible for the higher peak position of Si 2p when the PLA samples are dissolved in aqueous solution. For the chemical composition of PLA with different calcination temperatures (Table 1), measurements of the Al 2p lines detected by XPS fluctuated and had significant noise because of low Al content, so fitting lines were added to the figure. The charged environment with an octahedrally coordinated Al ion is more polarizable than that with a tetrahedrally coordinated Al ion. The Al 2p binding energy of an octahedrally coordinated Al ion is in the range from 74.1 to 75.0 eV, whereas the binding energy of a tetrahedrally coordinated Al ion varies from 73.4 to 74.55 eV (Black et al 2003). The binding energies for Al 2p line peaks of PLA-500, PLA-700, and PLA-850 are situated at approximately 73.86, 73.76, and 73.90 eV, respectively. The Al 2p lines for PLA are related to tetrahedrally coordinated ions. When the PLA samples were dissolved in aqueous solution, the peak position of Al 2p shifted toward higher binding energies located at approximately 74.52, 74.48, and 74.12 eV for PLA samples with different calcinations temperatures, which indicated

that some tetrahedrally coordinated Al ions transformed into octahedrally coordinated bonds.

## CONCLUSIONS

1. The specific surface area decreased, and median particle diameter increased with increasing calcination temperature. The dominant components of silica, potassium, magnesium, and calcium were observed in PLA. For the value of conductivity, PLA-850 had the highest, PLA-700 was moderate, and PLA-500 was the lowest. For the acid–base property, PLA-850 had strong alkalinity, PLA-700 was moderate, and PLA-500 was the weak alkalinity.
2. The zeta potential of PLA was calculated to be a negative value, and the zeta potential for PLA-850 changed slightly with increasing dissolution time. The absolute value of the zeta potential increased and then decreased with increasing dissolution time for PLA-500 and PLA-700.The SEM results showed that as the thermal temperature increased, the quantity of irregularly shaped materials decreased, and a more compact structure was observed in PLA samples.
3. Major mineral components were identified by XRD. Calcite and potassium sulfate can be found in the PLA-500 and PLA-700 samples, whereas magnesite and lime are easily identified in the PLA-850. When the PLA samples were dissolved in aqueous solution, the soluble minerals, such as lime and potassium sulfate, disappeared from the XRD results. For PLA-850, Si- and Al-containing minerals could be found. From the XPS analysis, the Si 2p peak was located at a lower position because of additional Si-OH synthesized with increasing calcination temperature. The Al 2p line for PLA is related to tetrahedrally coordinated Al. When the PLA samples were dissolved in aqueous solution, the Si 2p and Al 2p lines in PLA residues located at higher peak positions corresponding to the PLA samples. Overall, because of its low chemical activity and low zeta potentials, PLA is not recommended for use in cement systems.

## ACKNOWLEDGMENTS

This work was supported by the Joint Research Fund under a cooperative agreement between the NSFC and Funds for Coal-Based Low-Carbon Technology of Shanxi (No. U1710258 and U1810120); the National Natural Science Foundation of China (No. 51574172 and 51804208); the Research Fund of The State Key Laboratory of Coal Resources and Safe Mining, CUMT (SKLCRSM18KF016); and the China Postdoctoral Science Foundation (2018M632423).

## REFERENCES

Akhtar N, Goyal D, Goyal A (2016) Physico-chemical characteristics of leaf litter biomass to delineate the chemistries involved in biofuel production. J Taiwan Inst Chem Eng 62:239-246.

Baxter LL, Miles TR, Miles JTR, Jenkins BM, Milne T, Dayton D, Bryers RW, Oden LL (1998) The behaviour of inorganic material in biomass-fired power boilers: Field and laboratory experiences. Fuel Process Technol 54: 47-78.

Biricik H, AkÖz F, Berktay I, Tulgar AN (1999) Study of pozzolanic properties of wheat straw ash. Cem Concr Res 29:637-643.

Black L, Garbev K, Stemmermann P, Hallam KR, Allen GC (2003) Characterization of crystalline C-S-H phases by X-ray photoelectron spectroscopy. Cem Concr Res 33(6): 899-911.

Bridgwater T (2006) Biomass for energy. J Sci Food Agric 86:1755-1768.

Bai X, Zhou X, Li Z, Ni J, Bai X (2017) Properties and applications of biochars derived from different biomass feedstock sources. Int J Agric Biol Eng 10(2):242-250.

Bostrom D, Skoglund N, Grimm A, Boman C, Ohman M, Brostrom M, Backman R (2012) Ash transformation chemistry during combustion of biomass. Energy Fuels 26:85-93.

Cociña EV, Frías M, Hernández-Ruiz J, Savastano H (2013) Pozzolanic behaviour of a bagasse ash from the boiler of a Cuban sugar factory. Adv Cem Res 25(3):136-142.

Demeyer A, Voundi Nkana JC, Verloo MG (2001) Characteristics of wood ash and influence on soil properties and nutrient uptake: An overview. Bioresour Technol 77: 287-295.

Dwivedi VN, Singh NP, Dasa SS, Singh NB (2006) A new pozzolanic material for cement industry: Bamboo leaf ash. Int J Phys Sci 1(3):106-111.

Etiegni L, Campbell AG (1991) Physical and chemical characteristics of wood ash. Bioresour Technol 37: 173-178.

Evangelou MWH, Deram A, Gogos A, Studer B, Schulin R (2012) Assessment of suitability of tree species for the

production of biomass on trace element contaminated soils. J Hazard Mater 209-210:233-239.

Feng G, Qi T, Wang Z, Bai J, Li Z (2018) Physical and chemical characterization of Chinese maize stalk leaf ash: Calcining temperature and aqueous solution. BioResources 14(1):977-995.

Firdaus MYN, Osman H, Metselaar HS, Rozyanty AR (2016) Preparation and characterization of active $SiO_2$ from *Cymbopogon citratus* ash calcined at different temperature. BioResources 11(1):2839-2849.

Font A, Soriano L, Moraes JCB, Tashima MM, Monzó J, Borrachero MV, Payá J (2017) A 100% waste-based alkali-activated material by using olive-stone biomass ash (OBA) and blast furnace slag (BFS). Mater Lett 203:46-49.

Givi AN, Rashid SA, Aziz FNA, Salleh MAM (2010) Assessment of the effects of rice husk ash particle size on strength, water permeability and workability of binary blended concrete. Constr Build Mater 24(11):2145-2150.

Hafshejani LD, Nasab SB, Gholami RM, Moradzadeh M, Izadpanah Z, Hafshejani SB, Bhatnagar A (2015) Removal of zinc and lead from aqueous solution by nanostructured cedar leaf ash as biosorbent. J Mol Liq 211:448-456.

Jordan CA, Akay G (2012) Speciation and distribution of alkali, alkali earth metals and major ash forming elements during gasification of fuel cane bagasse. Fuel 91:253-263.

Knudsen JN, Jensen PA, Dam-Johansen K (2004) Transformation and release to the gas phase of Cl, K, and S during combustion of annual biomass. Energy Fuels 18(5): 1385-1399.

Karim MR, Hashim H, Abdul RH (2016) Assessment of pozzolanic activity of palm oil clinker powder. Constr Build Mater 127:335-343.

Lima AT, Ottosen LM, Pedersen AJ, Ribeiro AB (2008) Characterization of fly ash from bio and municipal waste. Biomass Bioenerg 32:277-282.

Liu X, Shen Y, Lou L, Ding C, Cai Q (2009) Copper tolerance of the biomass crops elephant grass (*Pennisetum purpureum* Schumach), vetiver grass (*Vetiveria zizanioides*) and the upland reed (*Phragmites australis*) in soil culture. Biotechnol Adv 27:633-640.

Ljiljana MK, Snežana SN, Miloš TN, Nenad KB, Bratislav ŽT, Vladimir BP, Zlatko LR (2017) Structural and chemical properties of thermally treated geopolymer samples. Ceram Int 43(9):6700-6708.

Liu Z, Tian D, Hu J, Shen F, Long L, Zhang Y, Yang G, Zeng Y, Zhang J, He J, Deng S, Hu Y (2018) Functionalizing bottom ash from biomass power plant for removing methylene blue from aqueous solution. Sci Total Environ 634:760-768.

Moghal AAB, Sivapullaiah PV (2012) Retention characteristics of $Cu^{2+}$, $Pb^{2+}$, and $Zn^{2+}$ from aqueous solutions by two types of low lime fly ashes. Toxicol Environ Chem 94(10):1941-1953.

Moraes JCB, Akasaki JL, Melges JLP, Monzó J, Borrachero MV, Soriano L, Payá J, Tashima MM (2015) Assessment of sugar cane straw ash (SCSA) as pozzolanic material in blended Portland cement: Microstructural characterization of pastes and mechanical strength of mortars. Constr Build Mater 94:670-677.

Paparazzo E, Fanfoni M, Severini E, Priori S (1992) Evidence of Si-OH species at the surface of aged silica. J Vac Sci Technol A 10(4):2892-2896.

Qu J, Zhang Q, Xia Y, Cong Q, Luo C (2015) Synthesis of carbon nanospheres using fallen willow leaves and adsorption of Rhodamine B and heavy metals by them. Environ Sci Pollut Res Int 22(2):1408-1419.

Steenari BM, Karlsson LG, Lindqvist O (1999) Evaluation of the leaching characteristics of wood ash and the influence of ash agglomeration. Biomass Bioenergy 16:119-136.

Simonsen ME, Sønderby C, Søgaard EG (2009) Synthesis and characterization of silicate polymers. J Sol Gel Sci Technol 50:372-382.

Shen J, Liu X, Zhu S, Zhang H, Tan J (2011) Effects of calcination parameters on the silica phase of original and leached rice husk ash. Mater Lett 65:1179-1183.

Soltani N, Bahrami A, Pech-Canul MI, González LA (2015) Review on the physicochemical treatments of rice husk for production of advanced materials. Chem Eng J 264: 899-935.

Ulery AL, Graham RC, Amrhein C (1993) Wood-ash composition and soil pH following intense burning. Soil Sci 156:358-364.

Vassilev SV, Baxter D, Andersen LK, Vassileva CG (2013a) An overview of the composition and application of biomass ash. Part 1. Phase–mineral and chemical composition and classification. Fuel 105:40-76.

Vassilev S, Baxter D, Vassileva C (2013b) An overview of the behaviour of biomass during combustion: Part I. Phase–mineral transformations of organic and inorganic matter. Fuel 112:391-449.

Vassilev SV, Baxter D, Christina G, Andersen LK, Vassileva CG (2014) An overview of the behaviour of biomass during combustion: Part II. Ash fusion and ash formation mechanisms of biomass types. Fuel 117:152-183.

Van LS, Koppejan J (2008) The handbook of biomass combustion and cofiring. Earthscan, London, UK and Sterling, VA. 442 pp.

Zhu J, Tang C, Wei J, Li Z, Laipan M, He H, Liang X, Tao Q, Cai L (2017) Structural effects on dissolution of silica polymorphs in various solutions. Inorg Chim Acta 471: 57-65.

Zhu Y, Hu J, Yang W, Zhang W, Zeng K, Yang H, Du S, Chen H (2018) Ash fusion characteristics and transformation behaviors during bamboo combustion in comparison with straw and poplar. Energy Fuels 32: 5244-5251.